

Microstructure and Wear Resistance of Fe-Based Amorphous Metallic Coatings Prepared by HVOF Thermal Spraying

Z. Zhou, L. Wang, D.Y. He, F.C. Wang, and Y.B. Liu

(Submitted February 9, 2010; in revised form August 24, 2010)

Amorphous metallic coatings with a composition of $\text{Fe}_{48}\text{Cr}_{15}\text{Mo}_{14}\text{C}_{15}\text{B}_6\text{Y}_2$ were fabricated by means of high velocity oxygen fuel (HVOF) thermal spraying process. The microstructure and wear performance of the coatings were characterized simultaneously in this article. It is found that the coatings present a dense layered structure with the porosity below 1.5%. The coatings primarily consist of amorphous matrix and some precipitated nanocrystals, though a fraction of Fe-rich phases and oxide stringers also formed during deposited process. High thermal stability enables the amorphous coatings to work below 920 K temperature without crystallization. Depending on the structural advantage, the amorphous coatings exhibit high average microhardness of 997.3 HV_{0.2}, and excellent wear resistance during dry frictional wear process. The dominant wear mechanism of amorphous coating under this condition is fatigue wear, leading to partial or entire flaking off of the lamellae. In addition, the appearance of oxidative wear accelerates the failure of fatigue wear.

Keywords Fe-based amorphous coating, HVOF, microstructure, wear

1. Introduction

During the last few decades, metallic glasses have attained an increasing interest of their unique combinations of physical and chemical properties. In the nineties, bulk metallic glasses (BMGs) with high glass forming ability (GFA) have been developed in a number of alloy systems (Ref 1-5), which required critical cooling rate of 1-100 K/s for glass formation with large dimensions ranging from millimeters to centimeters. However, these BMGs usually exhibit no plastic deformation after yielding and no work hardening during room temperature deformation due to the formation of highly localized shear bands (Ref 6-8), which significantly limits the range of possible applications as engineering and structural material. To avoid this disadvantage, these materials will be more attractive as

coatings to withstand aggressive environments according to their unusual attributes of wear and corrosion resistance (Ref 9, 10).

Over the last years, high velocity oxygen fuel (HVOF) thermal spraying has been used for depositing metals, cermets, and ceramics [Ref 11]. The deposited coatings have been widely used for industrial applications to alleviate wear or corrosion degree of the structural components, because they generally express low porosity, high hardness, low oxide content, high adhesion, and compression stress (Ref 12-15). Recently, for further demand of protective capability, some attempts have been made on preparation of amorphous alloy coatings by means of HVOF process (Ref 16-21), which seems more feasible due to its high cooling rate of 10^7 - 10^{10} K/s (Ref 22). Among the different alloy systems being researched, Fe-based amorphous metallic glasses are considered to be extremely viable candidates as surface protective coatings owing to their high crystallization temperature, superior corrosion and wear resistance, good magnetic properties, and relatively low material cost (Ref 23-25).

However, amorphous phase is a non-equilibrium phase, so alloys with high GFA would be favorable for forming high amorphous fraction coatings via thermal spraying processes. Up to now, a series of Fe-based BMGs with high GFA have been found in Fe-Cr-Mo-C-B alloy system (Ref 26), which supplies a better choice for fabricating relative amorphous metallic coatings. In this article, a $\text{Fe}_{48}\text{Cr}_{15}\text{Mo}_{14}\text{C}_{15}\text{B}_6\text{Y}_2$ alloy with high GFA (Ref 27) was selected to prepare amorphous coatings by HVOF spraying process. The microstructural characteristics of the amorphous coatings were investigated through several kinds of testing methods, and the microhardness, friction and wear behavior of the coatings were also examined subsequently.

This article is an invited paper selected from presentations at the 4th Asian Thermal Spray Conference (ATSC 2009) and has been expanded from the original presentation. ATSC 2009 was held at Nanyang Hotel, Xi'an Jiaotong University, Xi'an, China, October 22-24, 2009, and was chaired by Chang-Jiu Li.

Z. Zhou, and D.Y. He, College of Materials Science and Engineering, Beijing University of Technology, Beijing 100124, China; and Z. Zhou, L. Wang, F.C. Wang, and Y.B. Liu, School of Materials Science and Engineering, Beijing Institute of Technology, Beijing 100081, China. Contact e-mail: zhouzhengbjut@bjut.edu.cn.

2. Experimental Procedure

2.1 Materials Selection and Preparation

A $\text{Fe}_{48}\text{Cr}_{15}\text{Mo}_{14}\text{C}_{15}\text{B}_6\text{Y}_2$ master ingot was prepared from mixtures of pure Fe (99.9 mass%), Cr (99.9 mass%), Mo(99.9 mass%), C(99.9 mass%), Y(99.9 mass%) as well as pre-alloyed Fe-B (20.6 mass%) ingot by induction melting in a copper crucible under argon atmosphere. From the master alloy, fully amorphous ribbon samples of 0.05 mm thickness and 2 mm width were fabricated by a single-roller melt-spinning technique for calculating amorphous fraction of the powders and coatings. Powders of the same composition were produced by high pressure argon gas atomization method, and then sieved according to conventional sieve analysis and divided into different size ranges. The as-atomized powders with particle sizes in the range of 15-50 μm were used for spraying onto the 316L stainless steel substrates. All the substrates were degreased by acetone, dried in air, and then grit-blasted prior to deposition. The amorphous coatings with 400 μm thickness were prepared by JP5000 HVOF spraying system, and the detailed spraying parameters which had been optimized by an earlier work are presented in Table 1.

2.2 Microstructure Characterization

The microstructure of the powders and as-deposited coatings was characterized by scanning electron microscopy (SEM), energy dispersive spectroscopy (EDS), and transmission electron microscopy (TEM). Thin coating slices for TEM were first peeled from substrates by mechanical method and ground to about 50 μm , then thinned by ion-beam milling technique until perforation. X-ray diffraction (XRD) analysis of the specimens was performed on an x-ray diffractometer ($\text{Cu } K_\alpha$ radiation) with 2 θ diffraction angle ranging from 20 to 90°. Percentage of the porosity in the coatings was evaluated using image analysis on optical microscopy (OM). Oxygen content of the powders and detached coatings were analyzed by a Nitrogen/Oxygen determinator. The thermal stability and amorphous fraction of the samples was examined by differential scanning calorimeter (DSC) in a continuous heating mode at a rate of 0.33 K/s from room temperature to 1150 K under argon atmosphere.

2.3 Hardness and Wear Measurement

Vickers microhardness measurements were conducted on the cross section of the HVOF coatings with an applied

Table 1 Spraying parameters employed in the HVOF process

Parameter	Condition
HVOF gun system	Tafa JP5000 with 4" barrel
Kerosene flow, m^3/h	0.74
Oxygen flow, m^3/h	2.20
Feed rate, g/min	37.5
Spraying distance, mm	380
Traverse velocity, mm/s	500

load of 200 gf and indentation time of 15 s, and calculated as an average of 15 measurements. The dry friction and wear behavior of the amorphous coatings were determined using a ring on block tribometer. The material of frictional ring was GCr15 high carbon steel with a diameter of 49.22 mm. During total test duration of 15,000 cycles, the steel ring with a set rotational speed of 200 rpm, was pressed onto the surface of the fixed block where the amorphous coatings were deposited, under an applied load of 40 N. Before these tests, the coating surfaces were polished using wet grinding until 1200 grit SiC paper, ultrasonically cleaned in acetone, washed in distilled water, and dried in air for an hour to promote reproducible results. For comparison, 316L stainless steel substrates without surface amorphous coatings were also selected to perform the tests in the same way.

3. Results and Discussion

3.1 Coating Characteristic

The typical SEM image of the feedstock with diameters of 15-50 μm can be seen in Fig. 1. It is clearly that the majority of the particles produced by gas atomization in the argon atmosphere are spherical or near-spherical although some had small satellites attached, and most of them exhibit smooth surface as the meaning of good fluidity.

The XRD patterns of the atomized powders, melt-spun ribbon and as-deposited coatings are shown in Fig. 2. It is notable that a single broad halo peak appearing in all the samples indicates high amorphous phase content, which is primarily attributed to the high GFA of $\text{Fe}_{48}\text{Cr}_{15}\text{Mo}_{14}\text{C}_{15}\text{B}_6\text{Y}_2$ alloy system. The origin of the high GFA for this alloy is according to the three empirical rules for the achievement of high GFA (Ref 28). It is regarded that the alloy chosen here satisfies the three empirical rules for the stabilization of the supercooled liquid, leading to

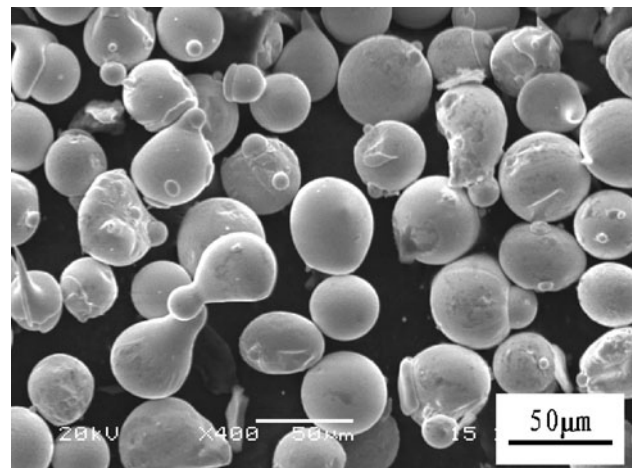


Fig. 1 A typical SEM image of $\text{Fe}_{48}\text{Cr}_{15}\text{Mo}_{14}\text{C}_{15}\text{B}_6\text{Y}_2$ alloy powders with 15-50 μm diameters

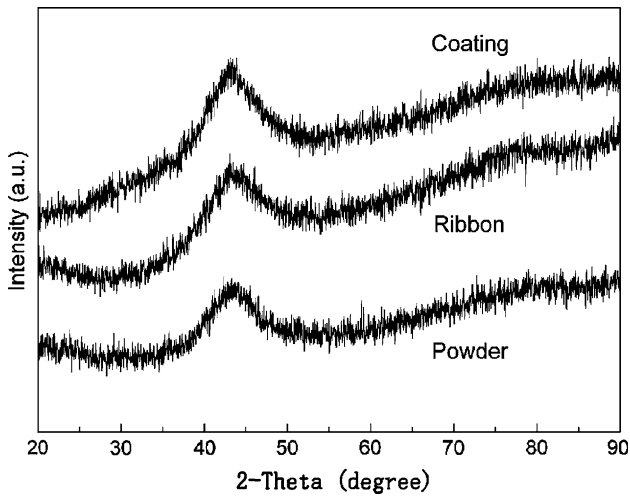


Fig. 2 XRD patterns of the melt-spun ribbon, atomized powders, and the as-deposited coatings

highly dense random packed atomic configurations, higher viscosity, and lower atomic diffusivity. The enhancement of atomic-level stress suppresses the nucleation and growth reactions of crystalline phases during devitrification, such as $(\text{Fe, Cr})_{23}\text{C}_6$ phase for the case of Fe-based BMGs with high carbon content (Ref 29). In addition, the high cooling rate of HVOF process also contributes to the formation of amorphous phase in the coatings.

The typical region from cross-sections of the coatings reveals its dense layered structure, as shown in Fig. 3, although some pores exist as very dark regions can be seen from the images. In general, the big pores located between flattened droplets are mainly caused by the loose packed layer structure or gas porosity phenomenon, while the small pores within the flattened particles originate from the shrinkage porosity (Ref 30). In despite of the presence of these defects, the coatings express a low porosity below 1.5% which is typical of HVOF thermal sprayed deposits. Also, it can be seen that a gradient in porosity exists across the thickness of the coatings, i.e., the top layers seem more porous and interfaces than the rest of the coating. This microstructural characteristic may therefore be significantly affected by the newly incoming particles with high velocity peening the previously deposited layers (Ref 31).

Furthermore, a fraction of heterogenous phases have been detected occasionally in the cross sections of the coatings after etching with aqua regia for seconds, as indicated in Fig. 4. Table 2 shows the EDS analysis for section A, B, and C marked in Fig. 4. It is clear that the distribution of primary elements at section A representing the most area of coatings is similar to that of the initial alloy system, though the content of boron and carbon is not accounted in which attributes to the resolving ability of EDS. However, the amount of Fe increases sharply to 82% (at.%) at section B, while Mo and Y are nearly exhausted, leading to these sections concerned as Fe-rich phase. The unmelted particles mainly consisted of Fe-rich phase are considered to appear owing to a fraction of non-uniform composition of the atomized powders, i.e., these

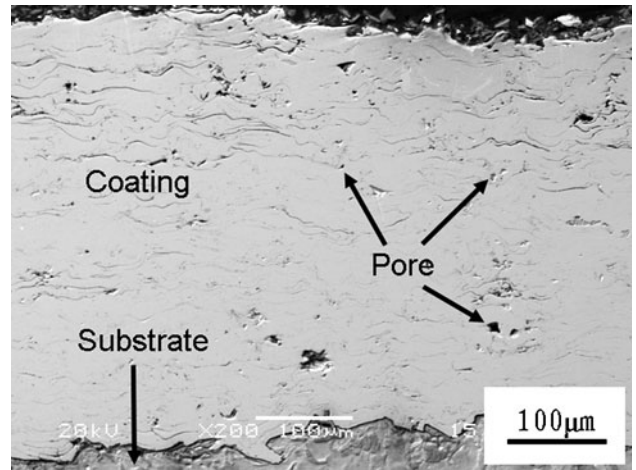
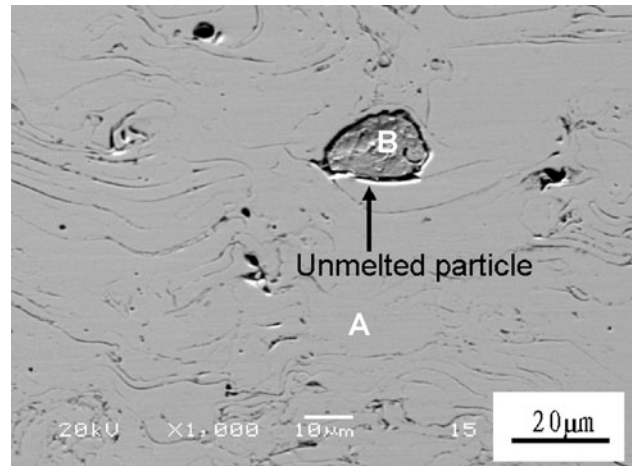
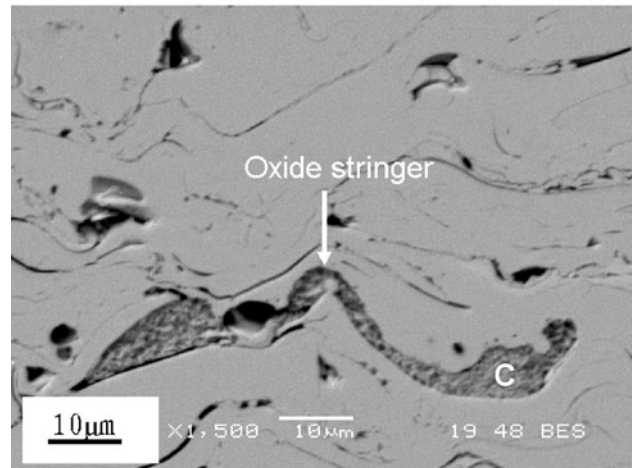


Fig. 3 SEM images of the entire cross-section of the as-deposited coatings



(a)



(b)

Fig. 4 Morphologies of the unmelted particle (a) and oxide stringer (b) within the as-deposited coatings

Table 2 EDS results (at.%) of section A, B, and C in Fig. 4 except boron and carbon

Section	Fe	Cr	Mo	Y	O
A	59.84	19.35	16.97	3.84	...
B	82.59	17.41
C	8.22	64.31	1.39	...	26.08

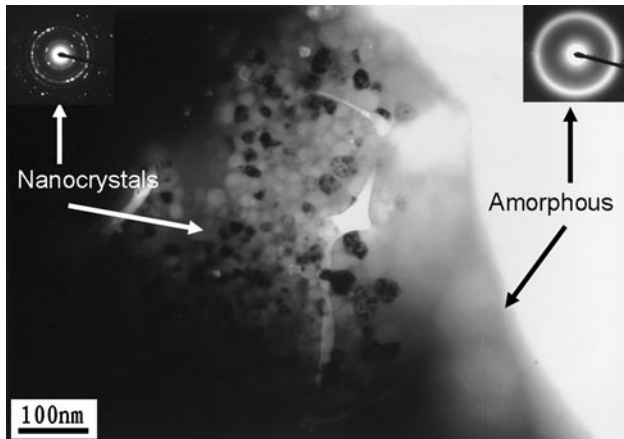


Fig. 5 Bright-field TEM image and selected area electron diffraction (SAED) patterns of the as-deposited coatings, including amorphous matrix and some nanocrystalline phase

particles formed during the production of original powders, but not for the deposited process, because the chemical constitution surrounding these particles is according with the designed alloy composition which manifests no evident diffusion of alloy elements. For the case of section C, which different from both section A and B, the content of Cr and O exhibits intensive increase compared with initial alloy composition, while the quantity of the other elements dramatically declines, so the main structure of these stringers can be ascertained as chromium oxide. It is regarded that some sprayed powders based on the situation of high temperature and excessive oxygen may form oxide layers on the outer sides of their surfaces during in-flight process. When the splats impact to substrate with subsequently flattened and spreading behavior, the oxide layer on the surface of particle is retained to form this lamellar structure (Ref 32). The oxygen content of the powders and the coatings are 0.06 and 0.25% (mass%), respectively, thus it could be concluded that slightly oxidation occurred during spraying process. Moreover, it is obvious that these heterogenous phases identified in Fig. 4 have all been eroded severely, whereas the surrounding amorphous matrix exhibits excellent corrosion resistance without evident change which belongs to their innate character and has been discussed widely elsewhere (Ref 24).

TEM was undertaken to obtain more detail information on microstructure formation of the coatings as shown in Fig. 5. The diffused halo rings in the selected area diffraction (SAD) pattern sited at the right corner of micrograph characterize that the coatings are primarily

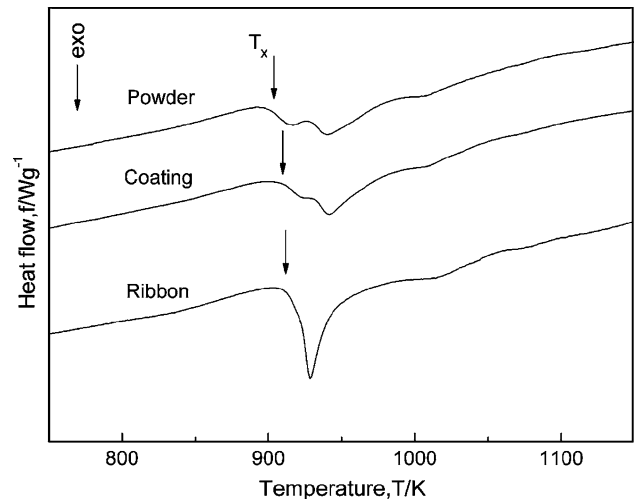


Fig. 6 DSC traces of the melt-spun ribbon, atomized powders, and the as-deposited coatings

composed of amorphous phase, which is according with the results of XRD examination. Nevertheless, some nanocrystalline grains, as can also be obviously ascertained in the micrograph, were precipitated in amorphous matrix with grain size in the range of 10-40 nm. The different result compared with XRD pattern may attribute to the limited ability of XRD determinator to detect the particular information of interior coatings. On the other hand, it validates that the generation of the nanocrystals is principally caused by heats accumulated inside the as-deposited coatings. To build up coatings with certain thickness, the spraying gun has to traverse over the previously deposited coatings, thus lots of overlapping and connecting lamellar splats formed coatings continuously. However, this operation leads to the localized reheating both from the direct effect of the gas jet and the latent heat evolutions as successive layers of melted splats solidified. As a result, it could be responsible for the formation of nanocrystalline grains originated from the amorphous matrix.

To clarify the amorphous content of the as-deposited coatings quantitatively, DSC traces of the coatings, powders, and ribbon were examined as well as their crystallization enthalpy (ΔH), as can be seen in Fig. 6. The volume fraction of amorphous phase of the coatings and powders is calculated by comparing their ΔH values with that of the ribbon standard sample, which has been proved as fully amorphous structure previously (Ref 29). As a result, the amorphous fraction (am.%) of the coatings is higher than 78%, as shown in Table 3, according to the preceding conclusions that partial nanocrystals were precipitated in amorphous matrix, and a small quantity of oxide stringers also formed during deposited process. However, the extremely high amorphous content of the present coating enables it to inherit the unique characteristics and properties of the BMGs. Moreover, it is interesting to detect that the amorphous fraction of the as-deposited coating exceeds the original powders. The generation of this unusual phenomenon may be owing to the relatively low

Table 3 Crystallization temperature (T_x), crystallization enthalpy (ΔH), and amorphous fraction (am.%) of the ribbon, powders, and coatings obtained by thermal analysis

Specimen	T_x , K	ΔH , J/g	Am.%
Ribbon	920.6	-65.57	100
Powder	916.8	-49.60	75.64
Coating	922.7	-51.36	78.32

spraying temperature and adequately tabular structure of the lamellae, leading to extremely high cooling rate generated during the solidification of droplets. Therefore, in this case, it could be much easier to obtain amorphous phase than gas atomization process. Nevertheless, as mentioned above, the successive spraying process has an adverse effect on the stability of amorphous phase, thus it can be concluded that the amorphous fraction of HVOF sprayed coatings is sensitive to spraying parameters. In addition, the onset crystallization temperature (T_x) of all the three samples are similar and exceed 915 K. That is to say, the coatings with high thermal stability against crystallization can be used in practice reliably and widely.

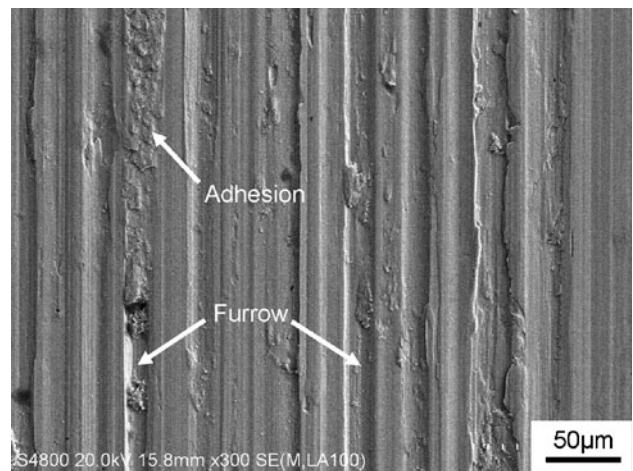
3.2 Hardness and Wear Resistance

The microhardness of Fe-based amorphous metallic coatings prepared by HVOF spraying process and 316L stainless steel substrates have been calculated and shown in Table 4. Obviously, the as-deposited coatings exhibit a significantly higher hardness than not only the 316L stainless steel, but also most of the crystal metallic alloys. The high hardness for amorphous coatings obtained now is mainly owing to their relatively high amorphous content, which has been validated by microstructural analysis conducted above. Also, it is one of the most attractive characteristics of the BMGs, in which the amorphous coatings have retained. In general, the extremely dense random packed atomic configurations of the amorphous structure can effectively resist the plastic deformation arose by applied load, thus leading to the high hardness performance of the amorphous coatings. In addition, the dispersion strengthening of nanocrystals precipitated in amorphous matrix, also contributes to the high hardness of as-deposited coatings.

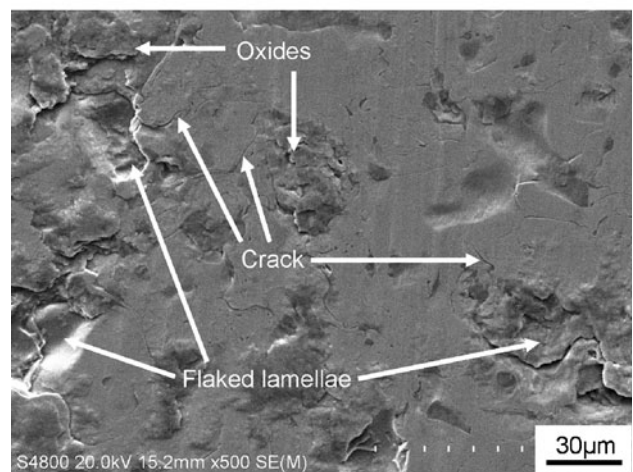
The wear resistance under dry frictional wear condition of amorphous coatings had been evaluated by calculating the weight loss after wear test using electronic balance with a limited accuracy of 0.1 mg. The results have been shown in Table 4, also in comparison with 316L stainless steel substrates. It is apparently that the as-deposited amorphous coatings exhibit extremely low wear loss and a relatively excellent wear resistance under this dry frictional wear condition. The relative wear resistance of amorphous coatings, which is inversely proportional to wear weight loss, can achieve approximately 47 times higher than that of the substrate material. Therefore, these amorphous coatings can be an effective and economic approach to protect substrates withstanding frictional wear environment and distinctly extending their lifetime.

Table 4 Microhardness and weight loss after wear test of the amorphous coatings, in comparison with 316L stainless steel

Specimen	Microhardness, HV _{0.2}	Weight loss, mg
Coating	997.3 ± 100	1.1
316L	414.5 ± 50	52.0



(a)



(b)

Fig. 7 Worn surface morphologies of the 316L stainless steel (a) and the as-deposited coatings (b)

Worn surface morphologies of the amorphous coatings and substrates were examined to clarify their wear behavior during dry frictional wear condition, as can be seen in Fig. 7. For 316L stainless steel substrates, it is visibly that there are numerous plastic furrows formed on the contact surface after testing, which is consistent with microcutting mechanism. At the same time, the trace of adhesive wear can also be observed at some of the furrow bottom. Therefore, the main wear mechanisms of 316L stainless steel are microcutting and adhesion, and the morphology of wide and deep furrows supports the great wear loss of the substrate material. In contrast, the trace of

adhesive wear has not been detected on the contact surface of the amorphous coatings, and there can be seen only slight scratches along the sliding direction. Nevertheless, the generation and propagation of cracks could be detected apparently on their worn surface, which implies fatigue wear as the dominant wear mechanism of the amorphous coatings. It is regarded that the cracks may prefer to initiate and propagate along with the defective regions, such as pores or lamellar interfaces on the surface or subsurface of the amorphous coatings due to the effect of alternative load, and subsequently leads to partial or entire flaking off of the lamellae as indicated in Fig. 7. Moreover, oxidative wear were also ascertained to occur during testing process, which were agreed with the cause of frictional heat. Also, it is believed that the oxygen tends to diffuse along with the defects on the surface of coatings, including fatigue cracks mentioned previously, because of the high atomic activity of these regions. As a result, the appearance of interface oxidation accelerated the failure of fatigue wear. It is therefore concluded that the main wear mechanism under dry frictional wear condition of the amorphous coatings is fatigue wear accompanying with oxidative wear.

The friction coefficient of the amorphous coatings and 316L stainless steel substrates related to testing time were also monitored, and the curves have been revealed in Fig. 8. It is found that the friction coefficient of substrates presents a drastically fluctuant characteristic, which probably attributes to the alternation of adhesion and shear fracture. By contrast with the substrates, the amorphous coatings exhibit more stable friction coefficient throughout the total duration. It could be guessed that the amorphous coatings would keep slow and stable wear loss for even much longer service time. Therefore, the excellent wear resistance and stable frictional behavior, make the amorphous coatings to be an effective material for surface protection under dry frictional wear condition.

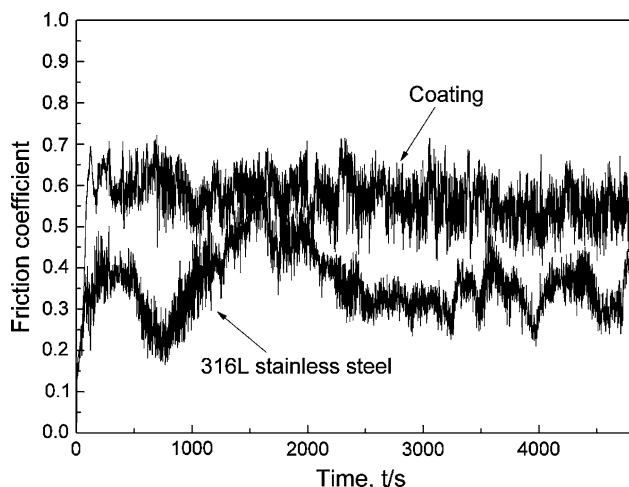


Fig. 8 Friction coefficient of the amorphous coatings and 316L stainless steel measured as a function of testing time

4. Conclusions

The results of the present study on the HVOF sprayed $\text{Fe}_{48}\text{Cr}_{15}\text{Mo}_{14}\text{C}_{15}\text{B}_6\text{Y}_2$ amorphous metallic coatings can be summarized:

- (1) The as-deposited coatings exhibit dense layered structure with the porosity below 1.5%. The coatings primarily consist of amorphous matrix due to both the high GFA of the alloy system and the high cooling rate of HVOF spraying process, and some nanocrystals resulting from recrystallization during successive spraying process. However, a fraction of Fe-rich phases originated from gas atomization process are retained as unmelted particles, and slight oxidation occurs during deposition. High thermal stability enables the amorphous coatings to work below 920 K without crystallization.
- (2) The amorphous coatings express high microhardness and extremely low weight loss during dry frictional wear test indicating a prominent ability of wear resistance, which mainly attributes to the relatively high amorphous content exceeding 78%. The dominant wear mechanism of amorphous coating under dry frictional wear condition is fatigue wear, leading to partial or entire flaking off of the lamellae. In addition, the appearance of oxidative wear accelerates the failure of fatigue wear.

References

1. A. Inoue, T. Zhang, and T. Masumoto, Production of Amorphous Cylinder and Sheet of $\text{La}_{55}\text{Al}_{25}\text{Ni}_{20}$ Alloy by a Metallic Mold Casting Method, *Mater. Trans. JIM*, 1990, **31**(5), p 425-428
2. T. Zhang, A. Inoue, and T. Masumoto, Amorphous Zr-Al-TM (TM=Co, Ni, Cu) Alloys With Significant Supercooled Liquid Region of Over 100 K, *Mater. Trans. JIM*, 1991, **32**(11), p 1005-1010
3. A. Peker and W.L. Johnson, A Highly Processable Metallic Glass: $\text{Zr}_{41.2}\text{Ti}_{13.8}\text{Cu}_{12.5}\text{Ni}_{10.0}\text{Be}_{22.5}$, *Appl. Phys. Lett.*, 1993, **63**(17), p 2342-2344
4. A. Inoue, T. Nakamura, N. Nishiyama, and T. Masumoto, Mg-Cu-Y Bulk Amorphous Alloys With High Tensile Strength Produced by a High-Pressure Die Casting Method, *Mater. Trans. JIM*, 1992, **33**(10), p 937-945
5. A.L. Greer, Metallic Glasses, *Science*, 1995, **267**(5206), p 1947-1953
6. T. Mukai, T.G. Nieh, Y. Kawamura, A. Inoue, and K. Higashi, Effect of Strain Rate on Compressive Behavior of a $\text{Pd}_{40}\text{Ni}_{40}\text{P}_{20}$ Bulk Metallic Glass, *Intermetallics*, 2002, **10**(11-12), p 1071-1077
7. D.V. Louzguine, H. Kato, and A. Inoue, High-Strength Cu-Based Crystal-Glassy Composite With Enhanced Ductility, *Appl. Phys. Lett.*, 2004, **84**(7), p 1088-1089
8. H. Choi-Yim, R. Busch, U. Koster, and W.L. Johnson, Synthesis and Characterization of Particulate Reinforced $\text{Zr}_{57}\text{Nb}_5\text{Al}_{10}\text{Cu}_{15.4}\text{Ni}_{12.6}$ Bulk Metallic Glass Composites, *Acta Mater.*, 1999, **47**(8), p 2455-2462
9. A.L. Greer, K.L. Rutherford, and I.M. Hutchings, Wear Resistance of Amorphous Alloys and Related Materials, *Int. Mater. Rev.*, 2002, **47**(2), p 87-112
10. D. Zander and U. Köster, Corrosion of Amorphous and Nanocrystalline Zr-Based Alloys, *Mater. Sci. Eng. A*, 2004, **375-377**(1-2), p 53-59
11. H. Herman, S. Sampath, and R. McCune, Thermal Spray: Current Status and Future Trends, *MRS Bull.*, 2000, **25**(7), p 17-25

12. S. Kuroda, Y. Tashiro, H. Yumoto, S. Taira, H. Fukanume, and S. Tobe, Peening Action and Residual Stresses in High-Velocity Oxygen Fuel Thermal Spraying of 316L Stainless Steel, *J. Therm. Spray Technol.*, 2001, **10**(2), p 367-374
13. M. Li and P.D. Christofides, Multi-scale Modeling and Analysis of an Industrial HVOF Thermal Spray Process, *Chem. Eng. Sci.*, 2005, **60**(13), p 3649-3669
14. A. Scrivani, S. Ianelli, A. Rossi, R. Groppetti, F. Casadei, and G. Rizzi, A Contribution to the Surface Analysis and Characterisation of HVOF Coatings for Petrochemical Application, *Wear*, 2001, **250-251**(Part 1), p 107-113
15. W.M. Zhao, Y. Wang, L.X. Dong, K.Y. Wu, and J. Xue, Corrosion Mechanism of NiCrBSi Coatings Deposited by HVOF, *Surf. Coat. Technol.*, 2005, **190**(2-3), p 293-298
16. F. Otsubo and K. Kishitake, Corrosion Resistance of Fe-16%Cr-30%Mo-(C, B, P) Amorphous Coatings Sprayed by HVOF and APS Processes, *Mater. Trans.*, 2005, **46**(1), p 80-83
17. D.J. Branagan, W.D. Swank, D.C. Haggard, and J.R. Fincke, Wear-Resistant Amorphous and Nanocomposite Steel Coatings, *Metall. Mater. Trans. A*, 2001, **32**(10), p 2615-2621
18. A.P. Wang, X.C. Chang, W.L. Hou, and J.Q. Wang, Preparation and Corrosion Behaviour of Amorphous Ni-Based Alloy Coatings, *Mater. Sci. Eng. A*, 2007, **449-451**(25), p 277-280
19. H. Choi, S. Yoon, G. Kim, H. Jo, and C. Lee, Phase Evolutions of Bulk Amorphous NiTiZrSiSn Feedstock During Thermal and Kinetic Spraying Processes, *Scr. Mater.*, 2005, **53**(1), p 125-130
20. M. Cherigui, N.E. Fenineche, and C. Coddet, Structural Study of Iron-Based Microstructured and Nanostructured Powders Sprayed by HVOF Thermal Spraying, *Surf. Coat. Technol.*, 2005, **192**(1), p 19-26
21. Y.P. Wu, P.H. Lin, G.Z. Xie, J.H. Hu, and M. Cao, Formation of Amorphous and Nanocrystalline Phases in High Velocity Oxy-Fuel Thermally Sprayed a Fe-Cr-Si-B-Mn Alloy, *Mater. Sci. Eng. A*, 2006, **430**(1-2), p 34-39
22. L. Li, B. Kharas, H. Zhang, and S. Sampath, Suppression of Crystallization During High Velocity Impact Quenching of Alumina Droplets: Observations and Characterization, *Mater. Sci. Eng. A*, 2007, **456**(1-2), p 35-42
23. A. Inoue, B. Shen, and C.T. Chang, Super-High Strength of Over 4000 MPa for Fe-Based Bulk Glassy Alloys in $[(Fe_{1-x}Co_x)_{0.75}B_{0.2}Si_{0.05}]_{96}Nb_4$ System, *Acta Mater.*, 2004, **52**(14), p 4093-4099
24. S.J. Pang, T. Zhang, K. Asami, and A. Inoue, Bulk Glassy Fe-Cr-Mo-C-B Alloys With High Corrosion Resistance, *Corros. Sci.*, 2002, **44**(8), p 1847-1856
25. A. Inoue, A. Makino, and T. Mizushima, Ferromagnetic Bulk Glassy Alloys, *J. Magn. Magn. Mater.*, 2000, **215-216**, p 246-252
26. V. Ponnambalam, S.J. Poon, G.J. Shiflet, V.M. Keppens, R. Taylor, and G. Petculescu, Synthesis of Iron-Based Bulk Metallic Glasses as Nonferromagnetic Amorphous Steel Alloys, *Appl. Phys. Lett.*, 2003, **83**(6), p 1131-1133
27. S.J. Pang, T. Zhang, K. Asami, and A. Inoue, Formation of Bulk Glassy $Fe_{75-x-y}Cr_xMo_yC_{15}B_{10}$ Alloys and Their Corrosion Behavior, *J. Mater. Res.*, 2002, **17**(3), p 701-704
28. A. Inoue, High Strength Bulk Amorphous Alloys With Low Critical Cooling Rates, *Mater. Trans. JIM*, 1995, **36**(7), p 866-875
29. V. Ponnambalam, S.J. Poon, and G.J. Shiflet, Fe-Based Bulk Metallic Glasses With Diameter Thickness Larger Than One Centimeter, *J. Mater. Res.*, 2004, **19**(5), p 1320-1323
30. V.V. Sobolev and J.M. Guilemany, Investigation of Coating Porosity Formation During High Velocity Oxy-Fuel (HVOF) Spraying, *Mater. Lett.*, 1994, **18**(5-6), p 304-308
31. T.C. Totemeier, Effect of High-Velocity Oxygen-Fuel Thermal Spraying on the Physical and Mechanical Properties of Type 316 Stainless Steel, *J. Therm. Spray Technol.*, 2005, **14**(3), p 369-372
32. J. Kim, K. Kang, S. Yoon, S. Kumar, H. Na, and C. Lee, Oxidation and Crystallization Mechanisms in Plasma-Sprayed Cu-Based Bulk Metallic Glass Coatings, *Acta Mater.*, 2010, **58**(3), p 952-962